Journal of Solid State Chemistry 184 (2011) 477–480

Contents lists available at ScienceDirect

Journal of Solid State Chemistry

journal homepage: www.elsevier.com/locate/jssc

Infrared, visible and ultraviolet absorptions of transition metal doped ZnS crystals with spin-polarized bands

J.H. Zhang [a], J.W. Ding [a,b,*], J.X. Cao [a,b], Y.L. Zhang [c]

[a] Department of Physics & Institute for Nanophysics and Rare-earth Luminescence, Xiangtan University, Xiangtan 411105, China
[b] Key Laboratory of Low Dimensional Materials & Application Technology, Xiangtan University, Xiangtan, Hunan 411105, China
[c] Department of Physics, Zhejiang University, Hangzhou 310027, China

ARTICLE INFO

Article history:
Received 14 July 2010
Received in revised form
6 November 2010
Accepted 28 November 2010
Available online 14 December 2010

Keywords:
TM:ZnS
Electronic structure
Optical property
Density functional theory

ABSTRACT

The formation energies, electronic structures and optical properties of *TM*:ZnS systems (*TM*=Cr^{2+}, Mn^{2+}, Fe^{2+}, Co^{2+} and Ni^{2+}) are investigated by using the first principles method. It is found that the wurtzite and zinc-blende structures have about the same stability, and thus can coexist in the *TM*:ZnS system. From the wurtzite *TM*:ZnS, especially, a partially filled intermediate band (IB) is obtained at *TM*=Cr^{2+}, Ni^{2+} and Fe^{2+}, while it is absent at *TM*=Mn^{2+} and Co^{2+}. The additional absorptions are obtained in infrared, visible and ultraviolet (UV) regions, due to the completely spin-polarized IB at Fermi level. The results are very helpful for both the designs and applications of *TM*:ZnS opto-electronics devices, such as solar-cell prototype.

1. Introduction

Zinc sulfide (ZnS) is an important II–VI semiconductor material of high optical quality, which has been used in opto-electronics devices, such as ultraviolet light-emitting diodes and injection lasers [1], flat panel displays [2] and infrared (IR) optical windows [3]. In the area of optics, it can be used as a reflector with high refractive index (2.35) and dielectric filter with high transmittance in the visible range [4,5]. Some new applications have also been found in photocatalysis [6] as a promising triboluminescent material [7,8]. For its potential applications, therefore, ZnS has attracted tremendous attention.

For pure ZnS crystal, the wurtzite structure of hexagon can be formed at high temperature [9], while it is less stable than zinc-blende of cubic lattice structure at room temperature. The wurtzite ZnS had been studied well both theoretically and experimentally. From the first-principles calculations, its electronic, optical and structural properties were well characterized [10]. Experimentally, Tran et al. [11] measured the photoluminescence properties of ZnS epilayers, from which bright band edge emission, including free exciton feature, was observed. For device development, importantly, dopants and impurities in ZnS can play an influential role in determining its electronic and optical properties.

Stern et al. [12] had theoretically studied the transition metals (*TM*) doped ZnS systems (*TM*:ZnS) with zinc blend structures by first principles. It is shown that for *TM*=Cr, Fe and Ni, the *TM*:ZnS systems can be half metallic, ferromagnetic, and 100% spin polarized from the densities of states (DOS) at Fermi energy, E_F. In such *TM*:ZnS systems, there exists Jahn–Teller effect on its optical transitions. By introducing a vibronic coupling to the Hamiltonian, Bevilacqua et al. [13] theoretically investigated Jahn–Teller effect on the emission and absorption spectra of Cr^{2+}:ZnS with the zinc-blende structure. It was shown that transitions happen between a $^5T_2$ ground multiplet and an excited ^5E multiplet in the near infrared region. Recently, more attention has been devoted to a laser material of Cr^{2+}:ZnS, which exhibits excellent lasing and optical properties in the mid-IR spectral region. Sorokina et al. [14] reported a room-temperature Cr^{2+}:ZnS laser with a continuously tunable waves of over 700 nm. By incorporating Mn^{2+} into ZnS, a wurtzite structure of Mn:ZnS system had also been obtained by Keller et al. [15], of which the absorption spectrum, *g* value and hyperfine splitting had been measured, showing an anisotropic behavior. Furthermore, the Cr:ZnS samples had been grown by both the physical vapor transport (PVT) method [16] and the chemical vapor transport method (CVT) [17], from which the mixed-polytype structures were observed. Such a structure demonstrates birefringence well. As one of the most structurally rich chalcogenide compounds, in fact, the mixed-polytype structures are common for *TM*:ZnS [18]. However, its formation mechanism is still unclear. Due to the limit computation capability, especially, the calculations of the mixed-polytype structures are very difficult. Even for the simple structures of both wurtzite and zinc-blende, their relative stabilities are not explored yet on the *TM*:ZnS systems. Therefore, the stability studies

* Corresponding author at: Department of Physics & Institute for Nanophysics and Rare-earth Luminescence, Xiangtan University, Xiangtan 411105, China.
E-mail address: jwding@xtu.edu.cn (J.W. Ding).

0022-4596/$ - see front matter © 2010 Elsevier Inc. All rights reserved.
doi:10.1016/j.jssc.2010.11.026

of *TM*:ZnS systems can contribute to the understanding of the mixed-polytype structures.

From the Cr:ZnS sample of zinc-blende structure, on the other hand, an intermediate band (IB) is found to be located between valence (VB) and conduction bands (CB) [19]. For a partially filled IB, it permits electrons transition from VB to IB and then to CB. This can lead to more efficient photons absorption of the solar-cell prototype than those by Shockley limit [20,21]. It is an interesting problem whether there exist IBs in other *TM*:ZnS systems at *TM*=Mn, Fe, Co and Ni, whether it is wurtzite or zinc-blende structure. For such *TM*:ZnS systems, the IB effect is far from clearly understood on the electrons transitions, and thus on their optical properties, which should be explored for the new high efficiency solar-cell prototype.

In this paper, we present a detailed investigation on the formation energies, electronic structures and optical properties of *TM*:ZnS systems (*TM*=Cr^{2+}, Mn^{2+}, Fe^{2+}, Co^{2+} and Ni^{2+}). In the presence of *TM*-doping, it is found that the stabilities of wurtzite structures of *TM*:ZnS systems are comparable to their zinc-blende structures, while the wurtzite structure of pure ZnS crystal is less stable than its zinc-blende structure. At *TM*=Cr^{2+}, Fe^{2+} and Ni^{2+}, a partially filled IB is found to be located between VB and CB, mainly due to the complete spin polarization of electrons at E_F, which is the appropriate characteristics of the new high efficiency solar-cell prototype. The absorption coefficients are then obtained, modulated remarkably by *TM*-doping, which are in good agreement with experiments. The results may be helpful for the design and application of the *TM*:ZnS opto-electronics devices.

2. Computational details

The formation energies of *TM*:ZnS are calculated using the VASP [22] code, and the electronic and optical properties of *TM*:ZnS are explored using the CASTEP code [23,24]. For both VASP and CASTEP, the generalized gradient approximation (GGA) of Perdew–Burke–Ernzerhof [25] (PBE) is chosen for parametrizing the exchange-correlation function. Kohn–Sham one-electron states are expanded in a plane wave basis set up to 350 eV. Brillouin zone integration is approximated by a sum over special k-points chosen using Monkhorst-Pack scheme [26], according to k-point spacing of 0.04 $Å^{-1}$ in all lattice directions. Due to *TM*-doping, spin polarization is considered in the calculations. For the VASP code, the calculations are performed with the PAW pseudopotentials [22]. At the end of the structural optimizations process, the residual Hellman–Feynman forces on the atoms are lower than 0.01 eV $Å^{-1}$. For CASTEP, the Ultrasoft pseudopotentials [27] are applied for all atoms when optimizing crystal geometries. Optimal atomic positions are determined until the magnitude of the forces acting on all atoms becomes <0.1 eV $Å^{-1}$. By this criterion, the geometry is optimized within 0.005 Å, leading to a convergence of the total energy within 0.05 meV. All the electronic structures and the optical properties are calculated upon the optimized geometries.

It is known that the dielectric function is mainly connected with the electronic response. The imaginary part $\varepsilon_2(\omega)$ of the dielectric function $\varepsilon(\omega)$ is calculated from the momentum matrix elements between the occupied and unoccupied wave functions, given by

$$\varepsilon_2 = \frac{ve^2}{2\pi\hbar m^2\omega^2}\int d^3\mathbf{k}\sum_{n,\,n'}|\langle \mathbf{k}n|\mathbf{p}|\mathbf{k}n'\rangle|^2 f(\mathbf{k}n)(1-f(\mathbf{k}n'))\delta(E_{\mathbf{k}n}-E_{\mathbf{k}n'}-\hbar\omega) \quad (1)$$

where $\hbar\omega$ is the energy of the incident photon, $\mathbf{p}$ is the momentum operator $(\hbar/i)(\partial/\partial x)$, ($|\mathbf{k}n\rangle$) is a crystal wave function and $f(\mathbf{k}n)$ is Fermi function. The real part $\varepsilon_1(\omega)$ of $\varepsilon(\omega)$ is evaluated from the imaginary part $\varepsilon_2(\omega)$ by Kramer–Kronig transformation. The absorption coefficient $I(\omega)$ can be derived from $\varepsilon_1(\omega)$ and $\varepsilon_2(\omega)$ as follows [28]:

$$I(\omega) = \sqrt{2}\omega\left[\sqrt{\varepsilon_1^2(\omega)+\varepsilon_2^2(\omega)}-\varepsilon_1(\omega)\right]^{1/2}, \quad (2)$$

which depends on $\varepsilon_1(\omega)$ and $\varepsilon_2(\omega)$, and thus on the energy. All other optical constants can also be obtained. Now, we can explore the optical properties of the ZnS and *TM*:ZnS systems.

3. Results and discussion

3.1. Formation energies

As a typical example, we create the supercell of wurtzite ZnS crystal, and then optimize its geometry. After optimizing the geometry, the system is on the ground state. The calculated lattice constants of pure ZnS are obtained to be $a=b=0.384$ and $c=0.630$ nm, which are different from previous theoretical results [29] of $a=b=0.334$ and $c=0.543$ nm, but in good agreement with the experimental result of $a=b=0.382$ and $c=0.626$ nm [30]. The results show that the calculations should be effective and reasonable.

To explore the stability of *TM*:ZnS systems, we use both the hexagonal phase of wurtzite structure and the cubic phase of zinc-blende structures. For initial lattice constants of the ZnS crystal, they are chosen to be $a=b=0.382$, $c=0.626$ nm, $\alpha=\beta=90^\circ$ and $\gamma=120^\circ$ for the hexagonal phase [30] and $a=b=c=0.5409$ nm, $\alpha=\beta=\gamma=90^\circ$ for the cubic phase [31]. In both phases, each Zn atom has four nearest-neighbor *S* atoms, and vice versa. To model *TM*-doping, one can replace one Zn atom in ZnS supercell with *TM* atom. The formation energies (E_{form}) for the doped systems are calculated by [32,33]

$$E_{(form)} = E_{(doped)} - [E_{(pure)} - E_{(Zn)} + E_{(TM)}] \quad (3)$$

where $E_{(doped)}$ and $E_{(pure)}$ are the total energies of the supercells with and without dopants, respectively. $E_{(Zn)}$ and $E_{(TM)}$ are the total energies of Zn and *TM* atoms in the ground state. For the wurtzite structures, here, we consider $2\times2\times2$ and $3\times3\times2$ supercells of 32 and 72 atoms, denoted as *w*-$TM_xZn_{1-x}S$ with $x=0.0625$ and 0.028, respectively. For the zinc-blende structures, we consider $2\times2\times1$ and $2\times2\times2$ supercells of 32 and 64 atoms, denoted as *z*-$TM_xZn_{1-x}S$ with $x=0.0625$ and 0.03125, respectively.

Table 1 shows the formation energies of both *w*-$TM_xZn_{1-x}S$ and *z*-$TM_xZn_{1-x}S$. Obviously, the formation energy of the Mn^{2+}:ZnS sample is the smallest in all the samples, whether it is the hexagonal phase or the cubic phase. Therefore, the Mn^{2+}:ZnS sample is more stable than other samples of *TM*=Cr^{2+}, Fe^{2+}, Co^{2+} and Ni^{2+}. This can be due to the fact that the half-filled 3*d* shell of Mn^{2+} acts as a complete shell [34,35], just as that in Zn^{2+}, which is different from other *TM* ions. For the same doping proportion ($x=0.0625$), especially, it is seen that both the wurtzite and zinc-blende structures of *TM*:ZnS have about the same formation energies. Different from the pure ZnS crystal, its zinc-blende structure is more stable than its wurtzite structure. Therefore, it is shown that the two structures of *TM*:ZnS have about the same stability, which may coexist in the *TM*:ZnS systems. This provides an explanation for the experimental observation of a mixed-polytype structure from a

Table 1
Formation energies of *w*-$TM_xZn_{1-x}S$ and *z*-$TM_xZn_{1-x}S$ (in units of eV).

Doped *TM* atoms	*w*-$TM_xZn_{1-x}S$		*z*-$TM_xZn_{1-x}S$	
	$x=0.0625$	$x=0.028$	$x=0.0625$	$x=0.03125$
Cr	−5.42	−5.33	−5.34	−5.31
Mn	−6.17	−6.17	−6.17	−6.18
Fe	−2.39	−2.30	−2.31	−2.30
Co	−1.31	−1.32	−1.36	−1.36
Ni	−4.72	−4.69	−4.74	−4.70

Cr^{2+}:ZnS sample [16]. In *TM*:ZnS of *TM*=Cr^{2+}, Fe^{2+}, Co^{2+} and Ni^{2+}, in addition, the formation energies of both *w*- and *z*-$TM_xZn_{1-x}S$ samples have a little increase with the doping proportion, while it is almost unchanged at *TM*=Mn^{2+}. This shows that the stability of the samples depends somewhat on the dopants and the doping proportion.

3.2. Electronic structures

For pure wurtzite ZnS, the obtained energy band is consistent with the previous result [10]. And a direct band gap of 2.17 eV is observed at the G point, smaller than 3.77 eV of the experimental result [36]. This is since the GGA theory generally underestimates the band gaps of insulators and semiconductors, due to the discontinuity of exchange–correlation energy [37]. Therefore, a scissors operator is introduced to shift all the conduction levels to agree with the measured value of the band gap [38–40]. In the present work, the scissors operator applied is 1.60 eV for pure ZnS and other semiconductor samples, accounting for the difference between the experimental band gap (3.77 eV) and the calculated band gap (2.17 eV). For the electronic and optical properties, we focus on the wurtzite structure of *TM*:ZnS systems. For the *w*-$TM_xZn_{1-x}S$ samples at $x=0.028$, we calculated its electronic structures for the various positions of *TM* dopant atoms. It is shown that the dopant positions have little influence on the band structures and DOS. In our calculations, one Zn atom bonding with four *S* atoms is chosen to be replaced. There are four isovalent positions for the replaced Zn atom in a supercell, of which the Zn atom at (0.44, 0.56 and 0.50) position is replaced by the *TM* atom.

Fig. 1 shows the total and partial DOS of $TM_xZn_{1-x}S$ at $x=0.028$ between −3 and 4 eV for *TM*=Cr (a), Mn (b), Fe (c), Co (d) and Ni (e). Solid, dotted and dashed lines represent the total DOS, the quintuplicate of *TM*-3*d* states and *S*-2*p* states. From Fig. 1, obviously, *S*-2*p* and *TM*-3*d* states are interdependent for all *TM*:ZnS systems, showing a covalent interaction existing between the *S* and *TM* atoms. In Fig. 1(a) of Cr^{2+}:ZnS, there are two main peaks of spin-up states, one locates at −0.79 eV and the other is at about E_F (−0.05 V). The results are similar to the previous work of its zinc-blende structure [41]. For Mn^{2+}:ZnS in Fig. 1(b), only one main peak of spin-up states is observed from the Mn^{2+}-3*d* state at −0.53 eV, but two main peaks of spin-down states are at 1.81 and 2.11 eV. Similar results can be observed from Co^{2+}:ZnS in Fig. 1(d), where two main peaks of spin-down states are observed from Co^{2+}-3*d* state at −0.29 and 0.71 eV. Therefore, it is shown that both Mn^{2+}:ZnS and Co^{2+}:ZnS are semiconductors and their spin polarization hardly happens at an E_F. In Fig. 1(c), interestingly, no main peak of spin-up states appears at about E_F, while there are two main peaks of spin-down states in Fe^{2+}-3*d* state, one at about E_F (−0.01 eV) and the other at 0.91 eV. Similar result is obtained from Ni^{2+}-3*d* state in Fig. 1(e), where two main peaks of spin-down states are observed, one is at about E_F (0.13 eV) and the other is at −0.68 eV. As a result, the spin polarization $P(E_F)$ at E_F are obtained to be 100%, −100% and −100% at *TM*=Cr, Fe and Ni, while $P(E_F)=0$ at *TM*=Mn and Co. For *TM*=Cr^{2+}, Fe^{2+} and Ni^{2+}, therefore, an isolated IB of 100% spin polarization appears at about E_F, located at between VB and CB. Thus, there exists a semiconductor-semimetal transition, just by doping of Cr^{2+}, Fe^{2+} and Ni^{2+}. The partially filled IB in those *TM*:ZnS systems permits electrons transition from VB to IB and then to CB, and thus leads to a more efficient photons absorption. The results indicate the potential applications of the *TM*:ZnS opto-electronics devices such as the new high efficiency solar-cell prototype.

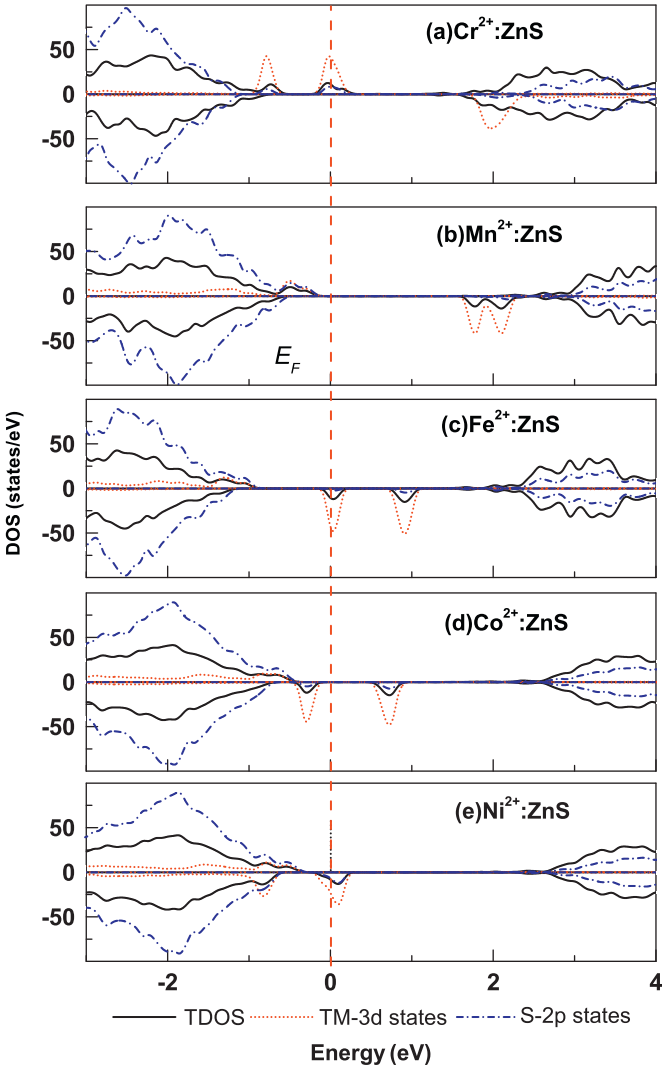

Fig. 1. DOS of *TM*:ZnS (*TM*=Cr^{2+}, Mn^{2+}, Fe^{2+}, Co^{2+} and Ni^{2+}); solid, dotted, dash-dotted lines represent the total DOS, the quintuplicate of *TM*-3*d* and *S*-2*p* states. Fermi level is indicated by a dash line.

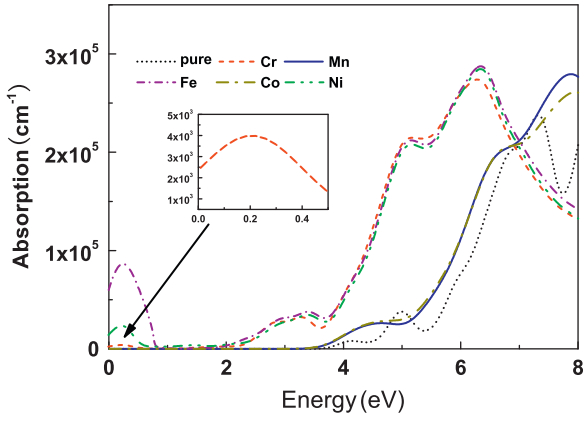

Fig. 2. Absorption coefficients of *TM*:ZnS crystals (*TM*=Cr^{2+}, Mn^{2+}, Fe^{2+}, Co^{2+} and Ni^{2+}).

3.3. Optical properties

In Fig. 2, we further show the absorption coefficients along the [1 0 0] direction for $TM_xZn_{1-x}S$ crystals at $x=0.028$. For a comparison, the absorption coefficient is also calculated for pure ZnS ($x=0$), in which there exists one main peak (at 7.32 eV) and one shoulder peak (at 5.01 eV). The absorption edge is obtained at about 3.63 eV, in agreement with the experimental value of 3.77 eV [36]. In case of *TM*:ZnS (*TM*=Cr^{2+}, Fe^{2+} and Ni^{2+}), a red shift is

observed for the absorption peak, which is different from pure ZnS. Except for the main peak at about 6.34 eV, three additional peaks appear at 0.22, 3.58 and 3.67 eV. The additional peak at about 0.22 eV is related to the IB of *TM*:ZnS (*TM*=Cr^{2+}, Fe^{2+} and Ni^{2+}). The peak values depend on the *TM*-doping, the biggest in an Fe:ZnS, next in an Ni:ZnS, and the lowest in Cr^{2+}:ZnS. In the visible region between 2.0 to 3.5 eV, especially, there appears a distinct additional absorption peak, due to the interband transition between *TM*-3*d* and *S*-2*p* conduction bands. Compared with pure ZnS, moreover the absorption coefficients of *TM*:ZnS systems are obviously increased, which are mainly ascribed to the *TM*-3*d* impurity states. Due to the intensive visible absorption, therefore, *TM*-doping may become a very important factor influencing the photocatalytic activity of ZnS, which would also make ZnS a potential candidate for solar-cell prototype. In addition, the UV absorption is enhanced in *TM*:ZnS systems, which could be applied in short-wavelength optoelectronic devices, such as UV detector and UV lightemitting diodes (LEDs). For *TM*=Mn^{2+} and Co^{2+}, the main peak appears at about 7.9 eV, two shoulder peaks at about 4.96 and 7.34 eV. The results show that the absorption coefficient can be remarkably modulated by *TM*-doping, indicating the potential applications of the *TM*:ZnS optical systems.

4. Conclusion

In the paper, the electronic structures and optical properties of *TM*:ZnS (*TM*=Cr^{2+}, Mn^{2+}, Fe^{2+}, Co^{2+} and Ni^{2+}) systems are studied by using the first principles method. It is found that the wurtzite and zinc-blende structures of a *TM*:ZnS system have about the same stability, while the wurtzite structure of pure ZnS is less stable than its zinc-blende one. Thus, the two structures can coexist in the system, which provides an explanation for the experimental observation of a mixed-polytype structure in Cr^{2+}:ZnS. Also, a partially filled IB is obtained between *TM*-3*d* and the conduction bands from the wurtzite *TM*:ZnS of *TM*=Cr^{2+}, Ni^{2+} and Fe^{2+}, while it is absent in Mn:ZnS and Co:ZnS. The IB electrons at Fermi level is completely spin-polarized, and thus leads to an additional absorption in the visible region. In addition, the absorption coefficients of *TM*:ZnS systems are calculated, from which an obvious red shift is observed. The results may be helpful for the design and applications of *TM*:ZnS devices, especially for the new high efficiency solar-cell prototype, UV detector and UV LEDs.

Acknowledgments

This work was supported by the National Natural Science Foundation of China (No. 10674113) and Foundation for the Author of National Excellent Doctoral Dissertation of China (Grant no. 200726).

References

[1] T. Yamamoto, S. Kishimoto, S. Iida, Physica B 308 (2001) 916–919.
[2] M. Bredol, J. Merikhi, J. Mater. Sci. 33 (1998) 471–476.
[3] P. Calandra, M. Goffredi, V.T. Liveri, Colloids Surf., A 160 (1999) 9–13.
[4] J.A. Ruffner, M.D. Himel, V. Mizrahi, G.I. Stegeman, U.J. Gibson, Appl. Opt. 28 (1989) 5209–5214.
[5] A.M. Ledger, Appl. Opt. 18 (1979) 2979–2989.
[6] T.A. Kennedy, E.R. Glaser, P.B. Klein, R.N. Bhargava, Phys. Rev. B 52 (1995) R14356–R14359.
[7] C.N. Xu, T. Watanabe, M. Akiyama, X.G. Zheng, Appl. Phys. Lett. 74 (1999) 2414–2416.
[8] O. Agyeman, C.N. Xu, M. Suzuki, X.G. Zheng, J. Mater. Res. 17 (2002) 959–963.
[9] B. Ray, II–VI Compd., Pergamon Press, Oxford, 1969.
[10] Y.N. Xu, W.Y. Ching, Phys. Rev. B 48 (1993) 4335–4351.
[11] T.K. Tran, W. Park, W. Tong, M.M. Kyi, B.K. Wagner, C.J. Summers, J. Appl. Phys. 81 (1997) 2803–2809.
[12] R.A. Stern, T.M. Schuler, J.M. MacLaren, D.L. Ederer, V. Perez-Dieste, F.J. Himpsel, J. Appl. Phys. 95 (2004) 7468–7470.
[13] G. Bevilacqua, L. Martinelli, E.E. Vogel, O. Mualin, Phys. Rev. B 70 (2004) 075206–075212.
[14] I.T. Sorokina, E. Sorokin, S. Mirov, V. Fedorov, V. Badikov, V. Panyutin, K.I. Schaffers, Opt. Lett. 27 (2002) 1040–1042.
[15] S.P. Keller, I.L. Gelles, W.V. Smith, Phys. Rev. 110 (1958) 850–855.
[16] I. Sorokina, E. Sorokin, S. Mirov, V. Fedorov, V. Badikov, V. Panyutin, K. Schaffers, Opt. Lett. 27 (2002) 1040–1042.
[17] I.T. Sorokina, E. Sorokin, S. Mirov, V. Fedorov, V. Badikov, V. Panyutin, A. Di Lieto, M. Tonelli, Appl. Phys. B 74 (2002) 607–611.
[18] T. Buch, B. Clerjaud, B. Lambert, P. Kovacs, Phys. Rev. B 7 (1973) 184–191.
[19] C. Tablero, Phys. Rev. B 74 (2006) 195203–195209.
[20] W. Shockley, H.J. Queisser, J. Appl. Phys. 32 (1961) 510–519.
[21] A. Luque, A. Martí, Phys. Rev. Lett. 78 (1997) 5014–5017.
[22] G. Kresse, D. Joubert, Phys. Rev. B 59 (1999) 1758–1775.
[23] M.D. Segall, P.J.D. Lindan, M.J. Probert, C.J. Pickard, P.J. Hasnip, S.J. Clark, M.C. Payne, J. Phys. Condens. Matter 14 (2002) 2717–2744.
[24] M.C. Payne, M.P. Teter, D.C. Allan, T.A. Arias, J.D. Joannopoulos, Rev. Mod. Phys. 64 (1992) 1045–1097.
[25] J.P. Perdew, K. Burke, M. Ernzerhof, Phys. Rev. Lett. 77 (1996) 3865–3868.
[26] H.J. Monkhorst, J.D. Pack, Phys. Rev. B 13 (1976) 5188–5192.
[27] D. Vanderbilt, Phys. Rev. B 41 (1990) 7892–7895.
[28] S. Saha, T.P. Sinha, A. Mookerjee, Phys. Rev. B 62 (2000) 8828–8834.
[29] P. Schröer, P. Krüger, J. Pollmann, Phys. Rev. B 47 (1993) 6971–6980.
[30] E. Kisi, M. Elcombe, Acta Crystallogr. C 45 (1989) 1867–1870.
[31] M. Rabadanov, Crystallogr. Rep. 40 (1995) 17–22.
[32] Z.Y. Zhao, Q.J. Liu, J. Phys. D: Appl. Phys. 41 (2008) 085417–085425.
[33] X.Y. Cui, J.E. Medvedeva, B. Delley, A.J. Freeman, N. Newman, C. Stampfl, Phys. Rev. Lett. 95 (2005) 256404–256407.
[34] K.C. Hass, H. Ehrenreich, J. Cryst. Growth 86 (1990) 8–14.
[35] J.K. Furdyna, J. Appl. Phys. 64 (1988) R29–R64.
[36] J.X. Ding, J.A. Zapien, W.W. Chen, Y. Lifshitz, S.T. Lee, X.M. Meng, Appl. Phys. Lett. 85 (2004) 2361–2363.
[37] Z. Lin, A. Orlov, R.M. Lambert, M.C. Payne, J. Phys. Chem. B 109 (2005) 20948–20952.
[38] J.H. Zhang, J.W. Ding, Y.L. Zhang, Solid State Commun. 149 (2009) 1188–1192.
[39] R. Asahi, T. Morikawa, T. Ohwaki, K. Aoki, Y. Taga, Science 293 (2001) 269–271.
[40] R.W. Godby, M. Schlüter, L.J. Sham, Phys. Rev. Lett. 56 (1986) 2415–2418.
[41] R.D. McNorton, T.M. Schuler, J.M. MacLaren, R.A. Stern, Phys. Rev. B 78 (2008) 075209–075211.